Postbuckling behaviour of beams with discrete nonlinear restraints

Finian McCann[1], M. Ahmer Wadee[2], Jack Pearson[3], Leroy Gardner[4]

Abstract

A beam with nonlinearly-elastic lateral restraints attached at discrete points along its span is investigated via analytical and numerical methods. Previous results for the critical moment and the deflected shape based on an eigenvalue analysis of a similar beam with linearly-elastic restraints are discussed, along with a validation of these results against an equivalent finite element model and results from numerical continuation. A beam with nonlinearly-elastic restraints is then analysed with treatments for both quadratic and cubic restraint force–displacement relationships being provided. After formulation of the potential energy functionals, the governing differential equations of the system are derived via the calculus of variations and appropriate boundary conditions are applied. The equations are then solved using the numerical continuation software AUTO-07p for a standard I-section beam. The variation in elastic critical buckling moment with the linear component of the restraint stiffness is tracked via a two-parameter numerical continuation, allowing determination of the stiffness values at which the critical buckling modes changes qualitatively. Using these stiffness values, subsequent analyses are conducted to examine the influence of the nonlinear component of the restraint stiffness, from which post-buckling equilibrium paths and deformation modes are extracted. The results of these analyses are then compared with an equivalent Rayleigh–Ritz formulation whereby the displacement components are represented by Fourier series. Equilibrium equations are derived by minimizing the potential energy functional with respect to the amplitudes of the constituent harmonics of the Fourier series. The amplitudes are solved for in the post-buckling range by AUTO-O7p and equilibrium paths are produced and compared to the equivalent solutions of the differential equations, with good agreement observed.

1. Introduction

The resistance of a beam against lateral-torsional buckling, an instability phenomenon involving lateral displacement and twisting of the cross-section of the beam, can be enhanced through the provision of restraints that inhibit either one or both of these deformations, thus increasing the overall load that the beam can safely support. Restraints can be continuous, like profiled metal sheeting, or discrete, like roof purlins. If they inhibit the amount of twist at a particular cross section, they are described as torsional

---

[1] Senior Lecturer in Structural Engineering, London South Bank University, <mccannf@lsbu.ac.uk>
[2] Professor of Nonlinear Mechanics, Imperial College London, <a.wadee@imperial.ac.uk>
[3] Undergraduate Student, Imperial College London, <j.pearson10@imperial.ac.uk>
[4] Professor of Structural Engineering, Imperial College London, <leroy.gardner@imperial.ac.uk>

restraints; if they inhibit the lateral displacement of the section, they are described as lateral restraints. The current work focuses on beams with discrete lateral restraints.

Initial studies of beams braced with single discrete lateral restraints were performed by Flint (1951) and Winter (1960). Trahair (1979), Trahair and Nethercot (1984) and Yura (2001) examined the stability of beams with continuous and lateral restraints through analytical and numerical methods, deriving critical lateral torsional buckling moments and buckling modes, and determined the stiffness and strength required of the bracing system to enforce particular buckling modes. In analysing a simply-supported beam of span L and depth between flange centroids h_s under constant bending moment M with a number n_b of linearly-elastic discrete braces of stiffness K at an arbitrary height a above the shear centre (see Fig. 1), McCann et al (2013) employed a Rayleigh–Ritz approach whereby the degrees-of-freedom, namely the lateral displacement of the shear centre u and the angle of twist of the cross-section ϕ were represented by Fourier sine series, along with the shape of the initial lateral imperfection e, which was necessary to include in order to obtain non-trivial equilibrium paths due to the linear nature of the model.
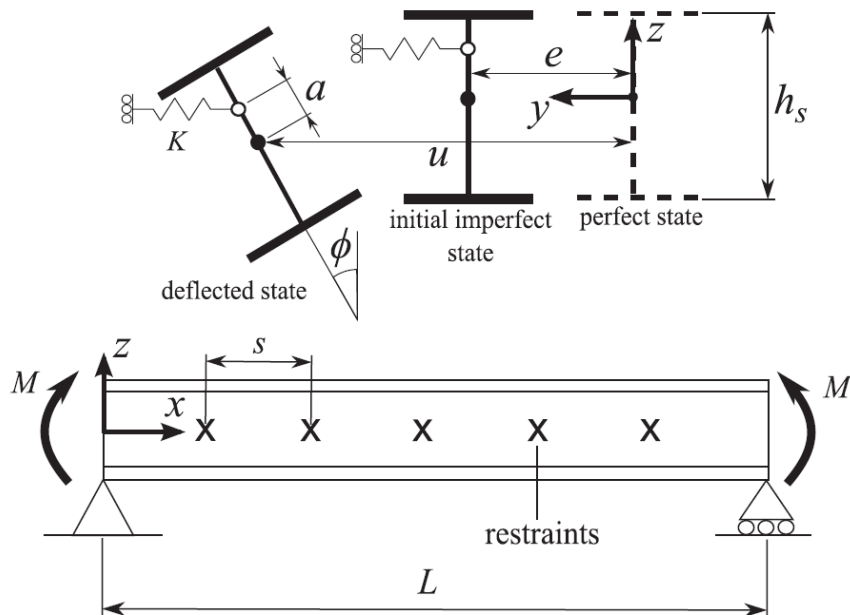

Figure 1: Cross-sectional geometry, system axes and configuration of the linearly-elastic model

Assuming small deflections (which is also assumed in the present study; nonlinearities are introduced via the force–displacement relationship of the restraints), the potential energy functional of the system was formulated. After performing a linear eigenvalue analysis of the system and applying difference calculus methods, expressions for the deflected shape, critical moment–restraint stiffness relationship and the stiffness required to force the beam to buckle in between the bracing nodes (the threshold stiffness) were derived.

After presenting a summary of the findings of McCann et al (2013) along with a validation of the analytical results against finite element and numerical continuation methods, the present study extends

the analysis to restraints with nonlinear force–displacement relationships. The analysis is based on variational principles whereby the total potential energy *V* of the system is given thus:

$$V = \frac{1}{2}\int_0^L \left[EI_z\left(u'' - e''\right)^2 + EI_w\phi''^2 + GI_t\phi'^2 + 2Mu''\phi\right]dx + \sum_{i=1}^{n_b}\int_0^{X_i}F(X^*)dX^* \tag{1}$$

where primes denote differentiation to the longitudinal ordinate *x*, EI_z, EI_w and GI_t are the minor axis flexural, warping and torsional rigidities, respectively, and the function *F*(*X*) is the force–displacement relationship for the restraints (where *X* is the restraint extension). In general, since small deflections are assumed:

$$X(x) = u(x) + a\phi(x) - e(x) \tag{2}$$

Since the restraints are at spacings of $L/(n_b + 1)$, the extension of the *i*th restraint X_i is given by:

$$X_i = u\left(\frac{iL}{n_b + 1}\right) + a\phi\left(\frac{iL}{n_b + 1}\right) - e\left(\frac{iL}{n_b + 1}\right) \tag{3}$$

2. Linearly-elastic restraints
McCann et al (2013) assumed the restraints to be linearly-elastic, such that:

$$F(X) = KX \tag{4}$$

and therefore the potential energy functional can be written:

$$V = \frac{1}{2}\int_0^L \left[EI_z\left(u'' - e''\right)^2 + EI_w\phi''^2 + GI_t\phi'^2 + 2Mu''\phi\right]dx + \sum_{i=1}^{n_b}\frac{1}{2}KX_i^2 \tag{5}$$

The lateral displacement of the shear centre, *u*, the angle of twist of the cross-section, ϕ, and the initial lateral imperfection *e* are represented by Fourier series, with the cosine terms set to zero to satisfy the fork support boundary conditions, thus:

$$u = \sum_n u_n \sin\left(\frac{n\pi x}{L}\right), \tag{6}$$

$$\phi = \sum_n \phi_n \sin\left(\frac{n\pi x}{L}\right), \tag{7}$$

$$e = \sum_n e_n \sin\left(\frac{n\pi x}{L}\right). \tag{8}$$

where u_n, ϕ_n and e_n are the amplitudes of the constituent harmonics of the respective series. Definition of *e* in this manner allows for any arbitrary initial imperfection to be included upon appropriate calibration of the values of e_n. Upon substitution of Eqs. (6) to (8) into Eq. (5) and evaluation of the integral, the harmonic amplitudes u_n and ϕ_n become the generalized co-ordinates of the system.

Equilibrium equations are derived by minimizing the system with respect to u_n and ϕ_n. From analysis of the resulting Hessian matrix $\mathbf{V_{ij}}$ of the system i.e. the matrix of second derivatives with respect to the generalized coordinates, it is found that there are two classes of buckling mode; an infinite number of modes where the beam buckles in between the restraints, and a finite number n_b of modes involving displacement of the bracing modes and interaction between certain sets of harmonics (McCann et al, 2013). Critical moments M_{cr} for the former class of modes are analogous to those of unbraced beams with a span equal to the restraint spacing $s = L / (n_b + 1)$, while for the latter class of modes the critical moment is determined implicitly through a closed-form expression for the brace stiffness K. Expressions describing the deformed shape of the beam and the threshold stiffness, K_T, required to force the beam to buckle in between the braces (termed full bracing) were also found.

In the remainder of this section, analytically-derived values for critical moment are compared with equivalent values found from finite element analysis, while the deflected shape of the beam is compared with equivalent results found via numerical continuation methods.

2.1 Validation of values for critical moment

A finite element model of a beam with discrete braces was developed in Abaqus (Abaqus, 2012) by Chrysos (2014), using open-section B31OS beam elements. Two beams were modelled, a 305×102×28 UB section beam of span 6.5 m and a 254×146×31 UB of span 5.25 m. Either three or four lateral restraints, modelled as linear springs, were attached along the beams. Linear eigenvalue (buckling) analyses were run for the cases of the braces being attached at the shear centre, at the compression flange and at a point half-way in between for a number of different restraint stiffnesses. The modelling of the braces located away from the shear centre was achieved by attaching a rigid link between the beam element and the spring element. Overall, there was very good agreement observed between the analytical and numerical results, as seen in the typical plot of restraint stiffness against critical moment shown in Fig. 2, thus validating the form of energy model. The values of stiffness and critical moment are normalized by the threshold stiffness K_T and the threshold moment M_T (the critical moment associated with full bracing), respectively.
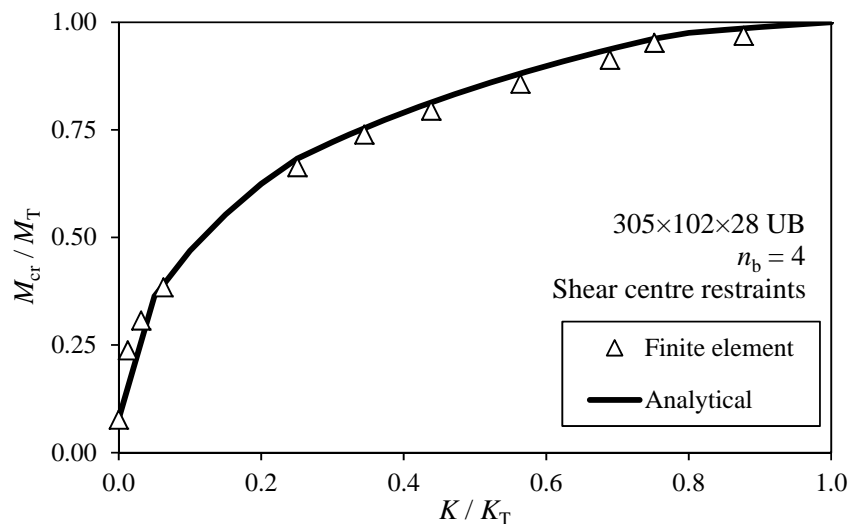

Figure 2: Typical comparison of numerical and analytical results from Chrysos (2014) for linearly-elastic model

4

2.2 Validation of results for deflected shape

In order to validate the results for deflected shape, the governing differential equations of the linear system were formulated initially using the calculus of variations (as performed by McCann (2012) and Hunt and Wadee (1998) previously) and normalized appropriately in order to be inputted for analysis by the numerical continuation software AUTO-07p (Doedel and Oldeman, 1997). In order to avoid computational difficulties associated with the restraint stiffness distribution being multi-valued at the bracing nodes, an equivalent piecewise-linear continuous stiffness distribution (McCann, 2012) was defined, such that the potential energy functional is fully continuous in *x* (see section 3.2).

The accuracy of the analytical method was assessed by calculating the coefficient of determination (R^2 value) between the analytically-derived deflected shapes and the equivalent results found by AUTO-07p. In total 720 cases were calculated, with over 86% of the results for *u* and ϕ having R^2 values of over 0.99, indicating a very high level of agreement between the two methods as shown in the example in Fig. 2.
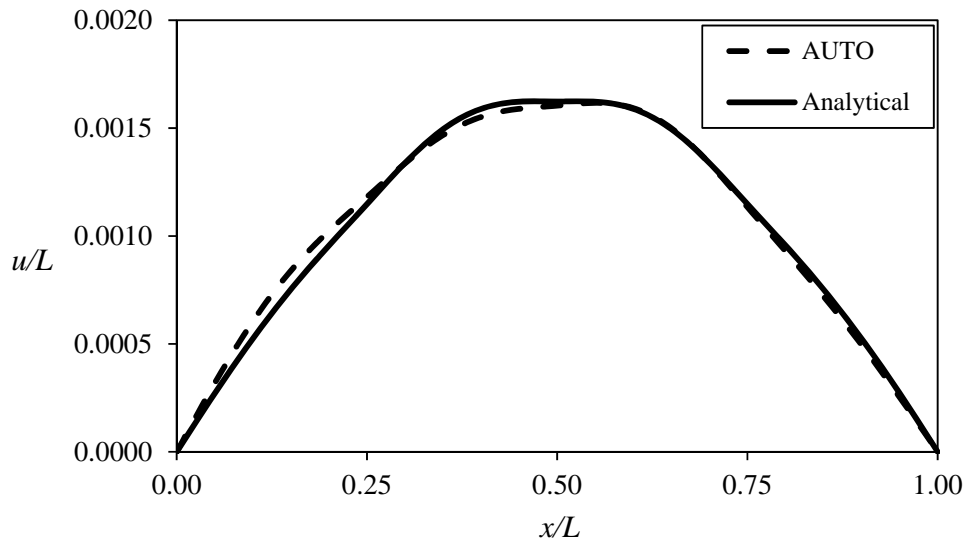

Figure 3: Typical comparison of analytical and numerical results for deflected shape for the linearly-elastic model

These comparisons provide satisfactory validation of the use of Fourier series in predicting the critical moment and deformed shape of beams with discrete linearly-elastic lateral restraints.

3. Analysis of nonlinear restraints

In this section, the analysis presented in section 2 is extended to beams with discrete lateral restraints that have nonlinear force–displacement relationships. The key enhancement offered by the nonlinear analysis is that, while in the linear analysis the behaviour of the system can only be described up to the bifurcation load (the critical moment), with the inclusion of the nonlinearity the postbuckling behaviour of the system can be examined. Since non-trivial equilibrium paths exist for the case of a perfect beam, in the remainder of the present study the lateral imperfection *e* is set equal to zero.

Two types of nonlinear restraint are examined: quadratic and cubic. After substituting the force–displacement relationship into the potential energy functional of Eq. (1), two methods of analysis are applied and compared. In the former, the governing differential equations of the system are derived via the calculus of variations and appropriate boundary conditions are applied. The numerical continuation software AUTO-07p is then used to solve for the displacement function directly using numerical

continuation, allowing the determination of postbuckling equilibrium paths and deflected shapes. In the latter, similar to the linear analysis of McCann et al (2013), the displacement functions are represented by Fourier series so that again the amplitudes of the constituent harmonics become the generalized coordinates of the system. However, closed-form solutions like those found by McCann et al (2013) for the case of linear restraints are difficult to obtain due to the inherent analytical complexity of the nonlinear models, and so AUTO-07p is used to solve for the harmonic amplitudes numerically.

3.1 Nonlinear restraint models

In the present study, a nonlinearity is introduced into the model by modelling the restraints as nonlinearly-elastic springs. Two force–displacement relationships for the springs are investigated, namely a quadratic softening spring, where:

$$F(X) = KX - C_2 X^2 \qquad (9)$$

and a cubic spring, where:

$$F(X) = KX - C_3 X^3 \qquad (10)$$

where C_2 and C_3 are the nonlinear components of the restraint stiffness for the quadratic and cubic springs, respectively. Typical force–displacement relationships for quadratic and cubic springs are shown in Fig. 4. It is important to note that both force-displacement relationships are softening, i.e., after a certain amount of displacement, the load-carrying capacity of the restraints reduces, thus eventually leading to unstable equilibrium. A practical example of a softening spring is a steel brace that eventually buckles under compression.
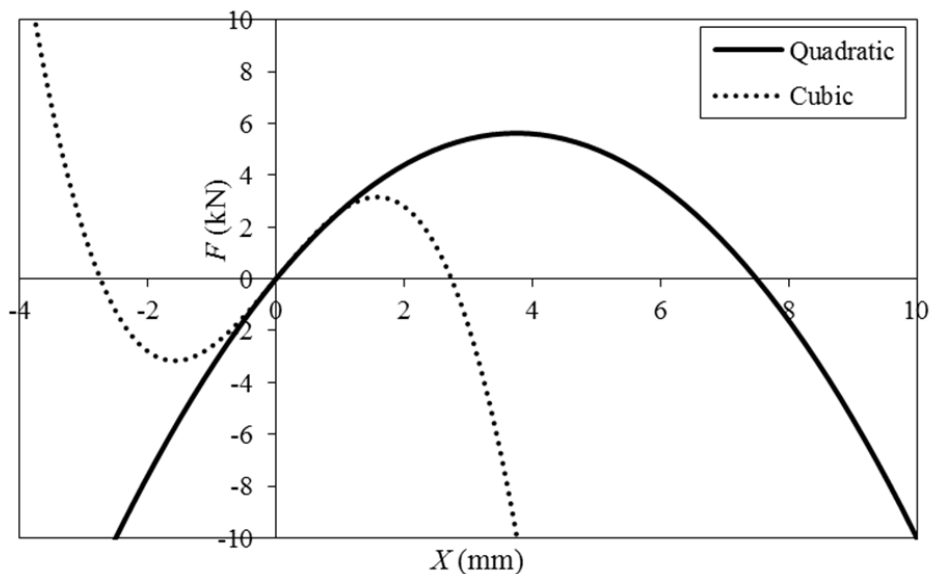

Figure 4: Typical force–displacement relationships for quadratic and cubic springs (K = 3000 N/mm, C_2 = 400 N/mm^2, C_3 = 400 N/mm^3)

The force–displacement relationships given in Eqs. (7) and (8) are substituted into the potential energy functional given by Eq. (1), so that the total potential energy for the quadratic spring model is given by:

$$V = \frac{1}{2}\int_0^L \left[EI_z u''^2 + EI_w \phi''^2 + GI_t \phi'^2 + 2Mu''\phi \right] dx + \sum_{i=1}^{n_b}\left(\frac{1}{2}KX_i^2 - \frac{1}{3}C_2 X_i^3 \right) \qquad (11)$$

while the total potential energy for the cubic model is given by:

$$V = \frac{1}{2}\int_0^L \left[EI_z u''^2 + EI_w \phi''^2 + GI_t \phi'^2 + 2Mu''\phi \right] dx + \sum_{i=1}^{n_b}\left(\frac{1}{2}KX_i^2 - \frac{1}{4}C_3 X_i^4 \right) \qquad (12)$$

With the total potential energy of the systems determined the two semi-analytical methods can be applied.

3.2 Calculus of variations
In contrast to the approach of McCann et al (2013) of solving for the displacement functions by representing them as infinite Fourier series and deriving expressions for the harmonic amplitudes, the displacement functions can also be solved for directly. For the nonlinear models this must be done via numerical methods due to analytical complexity inherent in the nonlinear potential energy functionals. The calculus of variations is used to derive the governing differential equations of the system; however, the potential energy functionals themselves must be fully continuous in order to derive the first variation and therefore the restraint energy terms outside the integrals in Eqs. (11) and (12) must be expressed as equivalent continuous functions. To this end, the following substitutions are made in the potential energy functionals for the quadratic and cubic models, respectively, for the restraint strain energy:

$$\sum_{i=1}^{n_b}\left(\frac{1}{2}KX_i^2 - \frac{1}{3}C_2 X_i^3 \right) \equiv \int_0^L \left(\frac{1}{2}kf(x)X(x) - \frac{1}{3}c_2 f(x)(X(x))^3 \right) dx \qquad (13)$$

$$\sum_{i=1}^{n_b}\left(\frac{1}{2}KX_i^2 - \frac{1}{4}C_3 X_i^4 \right) \equiv \int_0^L \left(\frac{1}{2}kf(x)X(x) - \frac{1}{4}c_3 f(x)(X(x))^4 \right) dx \qquad (14)$$

where $k = K/L$, $c_2 = C_2/L$, $c_3 = C_3/L$ and $f(x)$ is an equivalent continuous restraint stiffness distribution. This could assume a distribution of Dirac delta functions centred at the restraint nodes; however, this means that the function would be multi-valued at these points which would lead to computational difficulties in AUTO-07p. Instead, the distribution $f(x)$ comprises triangular distributions of stiffness about each bracing node and is defined such that the area underneath each piecewise-linear distribution is equal to L so that upon multiplication by, for example, k, the result is K. A typical form of $f(x)$ is given in Fig. 5. It was found by McCann (2012) that convergence was most reliable for a distribution base width of $L/50$.

For the sake of brevity, the derivation of the governing differential equations shall be shown here for the quadratic spring model only and in truncated form; a more complete treatment for both models is provided by Pearson (2014).

After substituting Eq. (13) into Eq. (11), for the quadratic model:

$$V = \int_0^L \left[\frac{1}{2} \left[EI_z u''^2 + EI_w \phi''^2 + GI_t \phi'^2 + 2Mu''\phi \right] + \frac{1}{2} kf(x)(u+a\phi) - \frac{1}{3} c_2 f(x)(u+a\phi)^3 \right] dx \quad (15)$$

The potential energy functional can now be expressed as a Lagrangian thus:

$$V = \int_0^L \mathcal{L}(u, u'', \phi, \phi', \phi'') \, dx \quad (16)$$

The first variation of the energy is given by:

$$\delta V = \int_0^L \left(\frac{\partial \mathcal{L}}{\partial u} \delta u + \frac{\partial \mathcal{L}}{\partial u''} \delta u'' + \frac{\partial \mathcal{L}}{\partial \phi} \delta \phi + \frac{\partial \mathcal{L}}{\partial \phi'} \delta \phi' + \frac{\partial \mathcal{L}}{\partial \phi''} \delta \phi'' \right) dx \quad (17)$$
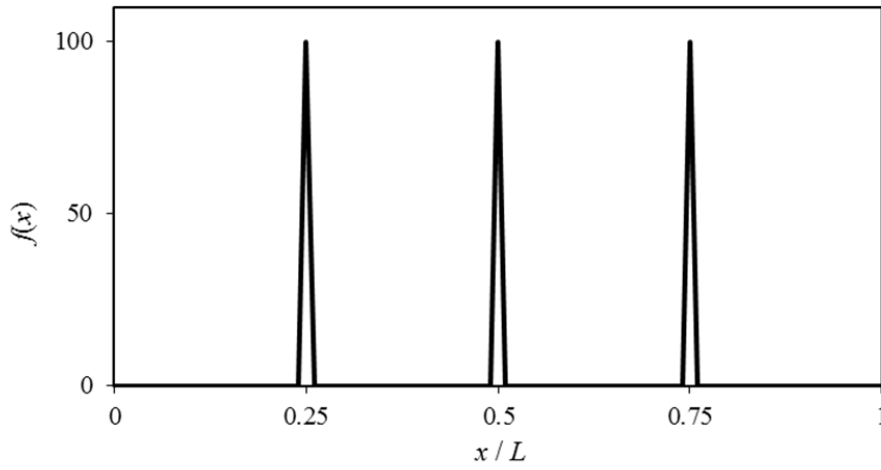

Figure 5: Stiffness distribution function $f(x)$ for a model with three restraints

By calculating the partial derivatives, performing integration by parts, applying appropriate boundary conditions and imposing equilibrium conditions by setting $\delta V = 0$ (Hunt and Wadee, 1998; McCann, 2012; Pearson, 2014), the coupled governing differential equations of the system are found:

$$u^{(4)} + \frac{M}{EI_z} \phi'' + \frac{kf(x)}{EI_z}(u+a\phi) - \frac{c_2 f(x)}{EI_z}(u+a\phi)^2 = 0 \quad (18)$$

$$\phi^{(4)} - \frac{GI_t}{EI_w} \phi'' + \frac{M}{EI_w} u'' + \frac{akf(x)}{EI_w}(u+a\phi) - \frac{ac_2 f(x)}{EI_w}(u+a\phi)^2 = 0 \quad (19)$$

Prior to input into AUTO-07p, the equations must be scaled and nondimensionalised appropriately. To this end:

$$\tilde{x} = x/L, \tilde{u}(\tilde{x}) = u(x)/L, \tilde{\phi}(\tilde{x}) = \phi(x), \tilde{f}(\tilde{x}) = f(x), \tilde{a} = a/L \quad (20)$$

8

and so the differential equations are:

$$\tilde{u}^{(4)} + \frac{ML}{EI_z}\tilde{\phi}'' + \frac{kL^4}{EI_z}\tilde{f}(\tilde{x})(\tilde{u}+\tilde{a}\tilde{\phi}) - \frac{c_2L^5}{EI_z}\tilde{f}(\tilde{x})(\tilde{u}+\tilde{a}\tilde{\phi})^2 = 0 \qquad (21)$$

$$\tilde{\phi}^{(4)} - \frac{GI_tL^2}{EI_w}\tilde{\phi}'' + \frac{ML^3}{EI_w}\tilde{u}'' + \frac{\tilde{a}kL^6}{EI_w}\tilde{f}(\tilde{x})(\tilde{u}+\tilde{a}\tilde{\phi}) - \frac{\tilde{a}c_2L^7}{EI_w}\tilde{f}(\tilde{x})(\tilde{u}+\tilde{a}\tilde{\phi})^2 = 0 \qquad (22)$$

4. Direct numerical solution of differential equations in AUTO-07p

With the differential equations formulated and submitted to AUTO-07p, numerical continuation analyses are run in order to provide solutions for the displacement functions. Pearson (2014) simulated, and presented results for, a 457 × 152 × 82 UB beam of span 9.3 m with from one to five restraints attached at the shear centre (i.e. $a = 0$) for both the quadratic and cubic models. In this section, the results for the model with three restraints is presented, which are representative of the overall behaviour of models with other numbers of restraints.

4.1 Variation of critical moment with linear component of stiffness

In the initial analysis, the stiffness terms are set equal to zero, allowing for the bifurcation moments of an unbraced beam to be solved for; the lowest of these is the elastic critical buckling moment M_{ob} of the unbraced beam. Next, a two parameter continuation is run from each of these bifurcation points whereby the change in critical moment of the braced beams with the linear component k of the equivalent distributed restraint stiffness is tracked.
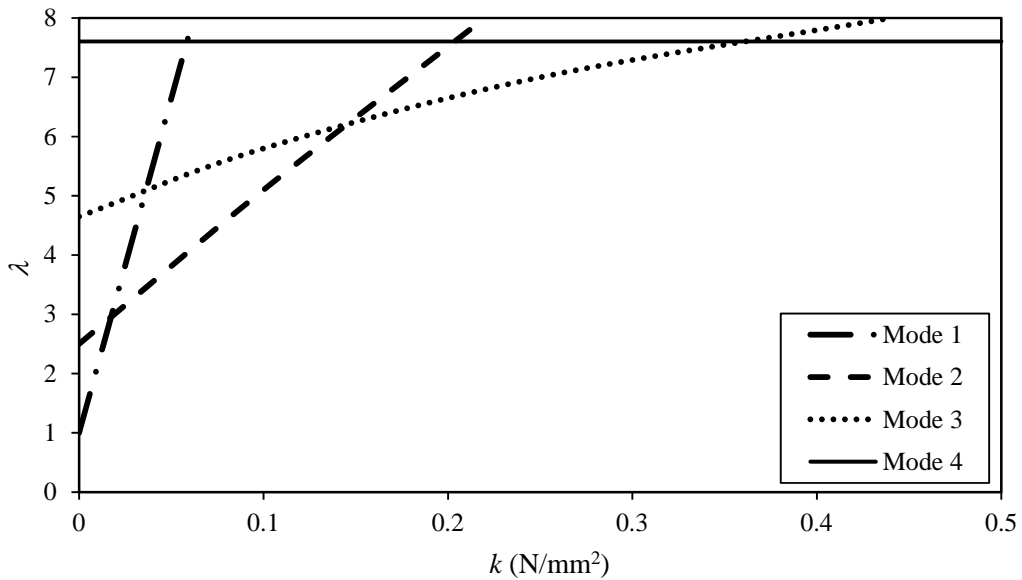

Figure 6: Results of two parameter continuation tracking change in critical moment (load parameter λ) with linear component of stiffness for a beam with three quadratic restraints.

In Fig. 6, results are shown of a such an analysis for a beam with three quadratic restraints, with load parameter $\lambda = M_{cr} / M_{ob}$ plotted against k. Along the vertical axis of Fig. 6, the initial bifurcation points for Modes 1 to 4 for the unbraced beam ($k = 0$) can be observed. Modes 1 to 3, in keeping with the findings of McCann (2012), are superpositions of particular sets of harmonics but are approximately

9

similar to single harmonics. Since there are three restraints, Mode 4 represents buckling in between the restraints, with no deflection of the bracing nodes, hence the lack of variation of critical moment with increasing restraint stiffness. It is noted that at this point, the nonlinear stiffness components have not been introduced, so the model is still linear and the equilibrium path is trivial, i.e. there is no displacement recorded prior to buckling.

4.2 Introduction of nonlinear stiffness component
The values of k at which the critical buckling mode transitions qualitatively are recorded. In Fig. 6, the transition from Mode 1 to Mode 2 occurs at approximately $k = 0.013$ N/mm^3, from Mode 2 to Mode 3 at $k = 0.141$ N/mm^3 and from Mode 3 to Mode 4 at $k = 0.349$ N/mm^3. Using these transition points as initial points, a further continuation is run whereby the nonlinear component c_2 (or c_3 for the cubic restraint model) of the stiffness relationship is introduced and the equilibrium paths are traced. Values of $c_2 = 3$ N/mm^3, 5 N/mm^3 and 6.4 N/mm^3 for the quadratic model (and $c_3 = 3$ N/mm^4, 5 N/mm^4 and 6.4 N/mm^4 for the cubic model) are used to investigate the influence of the strength of the nonlinearity.
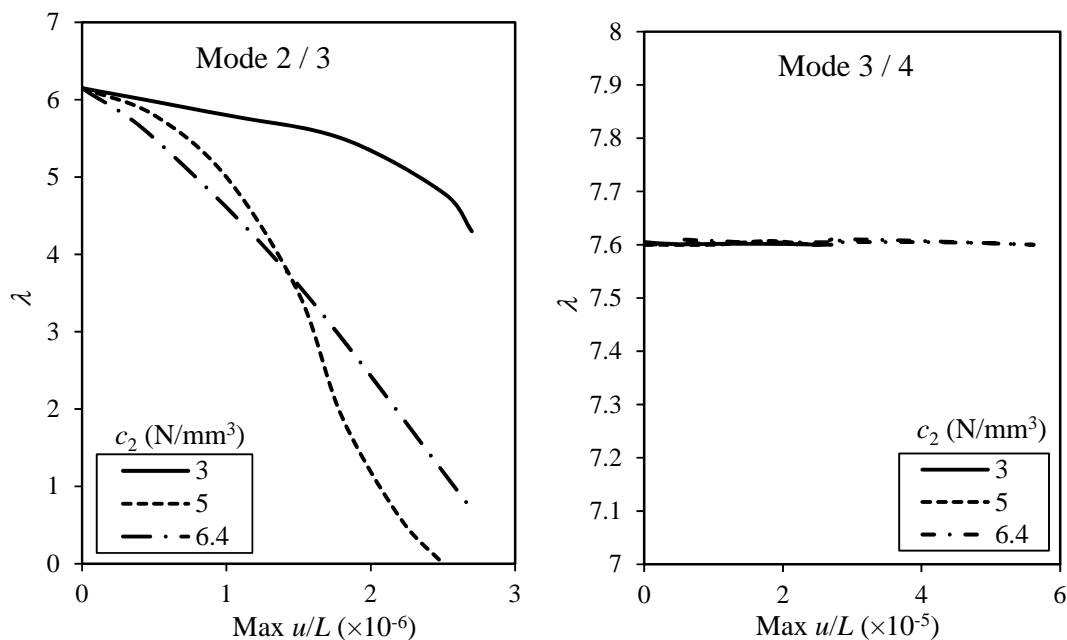

Figure 7: Equilibrium paths started at the modal intersection points for a beam with three quadratic restraints

In Fig. 7, equilibrium paths for a beam with three quadratic restraints are shown, with the load parameter λ being plotted against the normalized maximum lateral displacement across the beam span. In the left-hand plot of Fig. 7, where the runs have been started from the Mode 2 / 3 transition point, it can be seen that the system is in unstable equilibrium due to the softening springs and the load-carrying capacity reduces. It can also be seen that, initially, the strength (or lack of it) of the response is related to the strength of the nonlinearity. The curve with the smallest nonlinear component of $c_2 = 3$ N/mm^3 is associated with the least unstable postbuckling path, whereas the curves with higher values of c_2 display considerably more unstable behaviour. Interestingly, there exists a transition point at $\lambda = 3.87$ where the equilibrium path for $c_2 = 6.4$ N/mm^2 exhibits a stronger response than that for $c_2 = 5$ N/mm^2. It should be noted that this is not typical and in general the stronger nonlinearities produce a uniformly less stable response in other models.

10

In the right-hand plot of Fig. 7, where the equilibrium paths have been started from the Mode 3 / 4 transition, the influence of the lack of node displacement associated to Mode 4 can be seen. Since there is no node displacement, the introduction of the nonlinearity has no effect and in essence, there is a flat postbuckling response as would be seen in a linear analysis.

Mode shapes recorded along the equilibrium paths for c_2 = 6.4 N/mm^3 are shown in Fig. 8. For the paths started from the Mode 2 / 3 transition, it can be seen quite clearly that initially the dominant mode shape is the third harmonic; however, when progressing along the equilibrium path and with the load parameter decreasing, the mode shape transitions to one where the first mode is more dominant. This can be attributed to the reduction in energy available in the formation of the higher harmonics in the superposition of deformation modes. For the paths started from the Mode 3 / 4 transition, the mode shape is an almost pure Mode 4, with negligible displacement of the bracing nodes. Since there is (almost) no node displacement, the influence of the nonlinear component of the bracing stiffness is not activated and thus there is little to no variation in the load parameter, which is in agreement with the flat postbuckling response seen in Fig. 7.
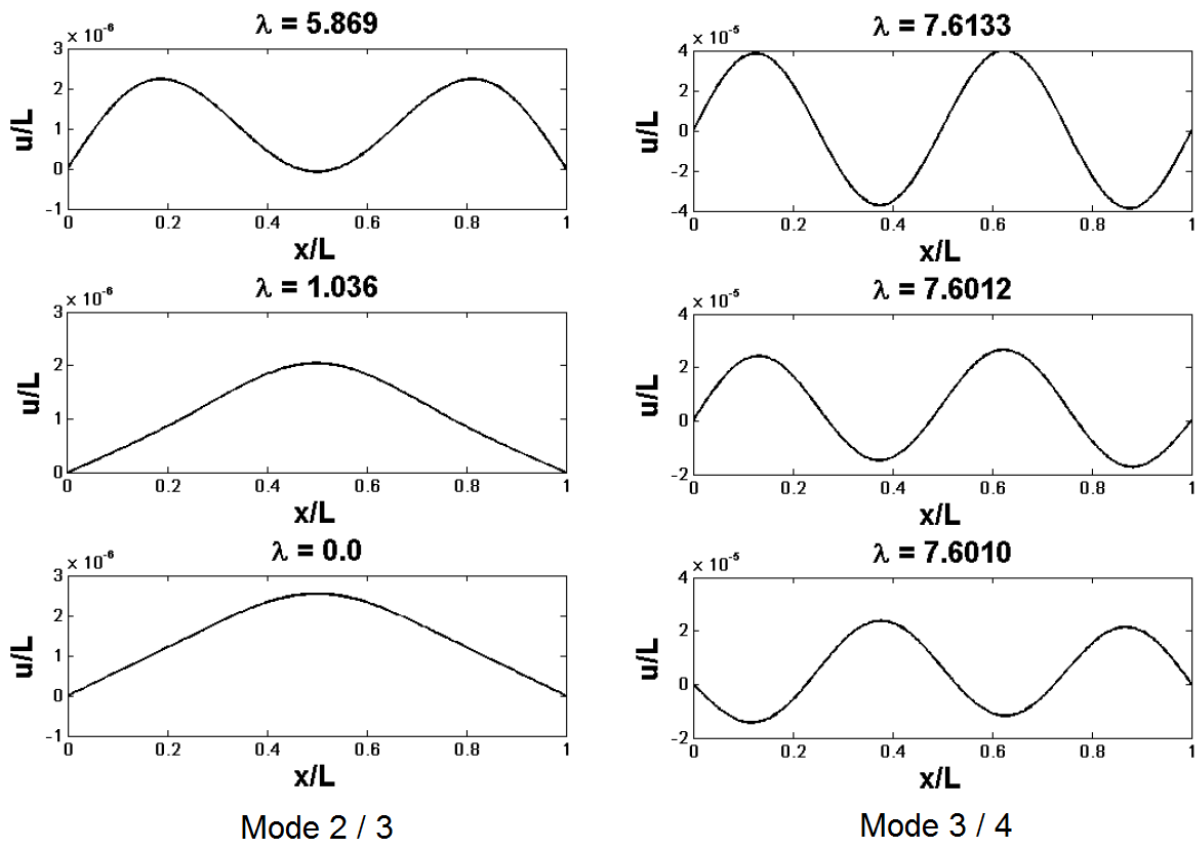

Figure 8: Mode shapes along the c_2 = 6.4 N/mm^3 equilibrium paths for a beam with three quadratic restraints

When comparing the results of the quadratic models and the cubic models, the form of the equilibrium paths are found to be quite similar overall. However, noticeable differences are apparent upon comparison of the mode shapes, as shown in Fig. 9. The mode shapes for the quadratic model are not symmetric since the stiffness responses are different depending on the sense of the extension of the

restraint, as shown in Fig. 4. In contrast, for the cubic model where the stiffness response is identical for both positive and negative extension, antisymmetric mode shapes are observed.
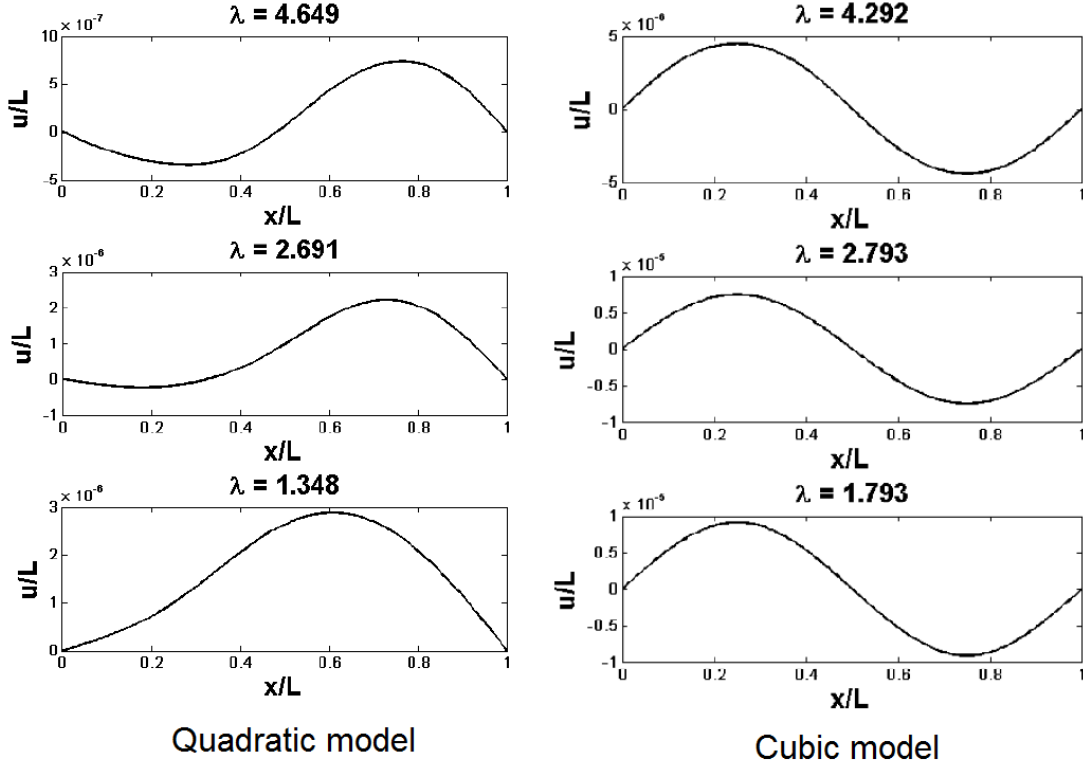

Figure 9: Comparison of mode shapes from the quadratic and cubic models

5. Rayleigh–Ritz analysis

In this section, comparison is made between solving the governing differential equations directly and a Rayleigh–Ritz analysis whereby the displacement functions u and ϕ are represented by Fourier series thus, as was done for the linear analysis of McCann et al (2013). In the linear analysis, infinite Fourier series were substituted into the potential energy formulation and closed-form expressions for the harmonic amplitudes were found analytically. For the nonlinear model, however, closed-form solutions are inhibited by the analytical complexity of the problem and thus AUTO-07p is used to solve for the harmonic amplitudes numerically; thus, the Fourier series are truncated to a finite number of terms. It was found by McCann (2012) that the Fourier series converge quickly and thus can be approximated quite well by only a few terms. In order to capture the full range of modes up to buckling in between the restraints, a total of $n_b + 1$ terms are employed, thus reducing the analytical complexity considerably:

$$u = \sum_{n=1}^{n_b+1} u_n \sin\left(\frac{n\pi x}{L}\right), \qquad (23)$$

$$\phi = \sum_{n=1}^{n_b+1} \phi_n \sin\left(\frac{n\pi x}{L}\right). \qquad (24)$$

The expressions are then substituted into the potential energy functionals of Eq. (11) for the quadratic model and Eq. (12) for the cubic model and the integration is carried out. Thus, the generalized

coordinates of the system are now the harmonic amplitudes u_n and ϕ_n and the equilibrium equations are found by minimizing the potential energy V with respect to the amplitudes:

$$\frac{\partial V}{\partial u_n} = 0,$$

(25)

$$\frac{\partial V}{\partial \phi_n} = 0.$$

(26)

Numerical solution of the equilibrium equations in AUTO-07p provides results for the harmonic amplitudes and thus the deformed shape of the beam upon superposition of the constituent harmonics.

5.1 Linear analysis
Initially, the stiffness components are set equal to zero, allowing the bifurcation points for an unrestrained beam to be solved for; as expected, it is found that the results are identical to those found through direct solution of the differential equations in AUTO-07p. In this section, although it is now no longer necessary to represent the restraint stiffnesses as distributed continuous functions since it is the harmonic amplitudes that are being solved for rather than the continuous displacement functions, values of $k = K / L$ and $c_2 = C_2 / L$ are reported in order to facilitate comparison with the results of Section 4.

Upon inclusion of the linear component of the stiffness and running a two parameter continuation tracking the variation of the critical moment with k, moment–stiffness curves are produced as shown in Fig. 10. For lower modes and at relatively lower stiffnesses, where the truncated Fourier series approximate the full solution well, there is good agreement between the curves and those found through direct solution of the differential equations. As the stiffness and critical mode increases, the contribution of higher harmonics to the full solution is more pronounced. Since the truncated series are lacking these higher harmonics, some discrepancies between the results of the two methods are observed. This trend is observed regardless of the number of restraints.
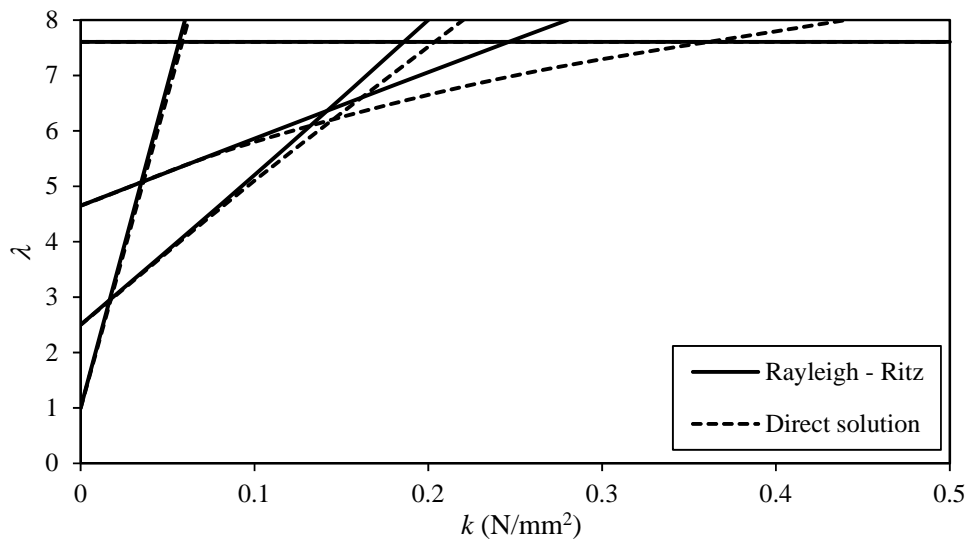

Figure 10: Comparison of moment–stiffness curves derived via the direct numerical solution and Rayleigh–Ritz methods for a beam with three linear restraints

5.2 Nonlinear analysis

With the inclusion of the nonlinear stiffness component, the harmonic amplitudes are found via numerical continuation and postbuckling equilibrium paths can be extracted. In Fig. 11 the load parameter λ is plotted against the various harmonic amplitudes u_n of the Fourier series approximating the lateral displacement, with the nonlinear analysis having been initiated from a point along Mode 2 of the linear analysis (k = 0.056 N/mm^2) with c_2 set at 5 N/mm^3. The change in the strength of the harmonics and the dominance of particular modes can be observed from these plots. Initially, at λ = 4, the second harmonic is dominant, with a similar contribution from the third harmonic in the positive sense. As the equilibrium path progresses and the moment decreases, the strength of the first harmonic increases continually. At λ = 2.8, the second and third harmonics begin to diminish until eventually at approximately λ = 2, the second and third harmonics vanish and the first mode becomes dominant. A superposition of first and third harmonics prevails after this point. It can be seen that, since the fourth mode does not involve any displacement of the bracing nodes, it is not active along the equilibrium path. It can be seen from the plots relating to the first and third harmonics that the response is not symmetric; this can be attributed to the non-symmetric nature of the quadratic force–displacement relationship. In the cubic model, symmetric equilibrium paths were observed for all modes.
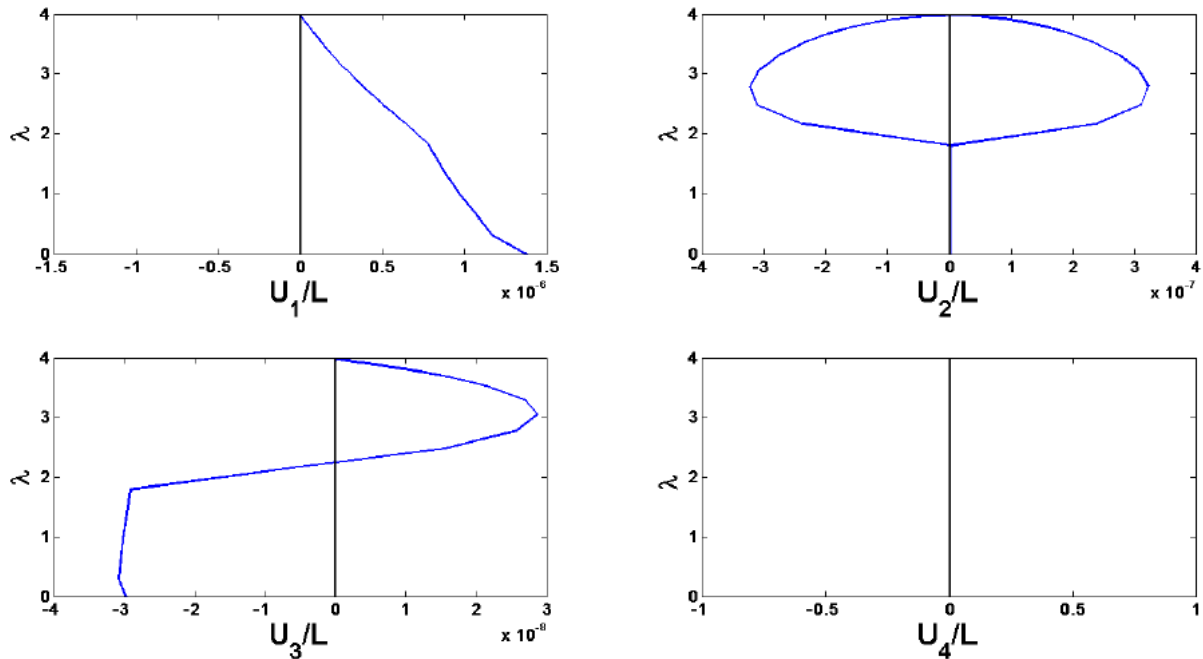

Figure 11: Equilibrium paths in terms of harmonic amplitudes for a beam with three quadratic restraints

5.3 Mode shapes

In Fig. 12, mode shapes obtained from the Rayleigh–Ritz analysis of a beam with three quadratic restraints are compared with those obtained from direct numerical solution of the governing differential equations across a range of linear stiffness starting points (with c_2 = 5 N/mm^3). It can be seen that the truncated Fourier series, while only comprising three harmonics, can capture the full mode shape quite accurately for the simulations started from Modes 2 and 3 of the linear analysis. When comparing the run started from Mode 4 of the Rayleigh-Ritz analysis, it can be seen that the third harmonic is dominant in the mode shape returned via direct numerical solution; this is commensurate with Fig. 10, where Mode 3 is the critical mode returned via direct numerical solution at this stiffness.
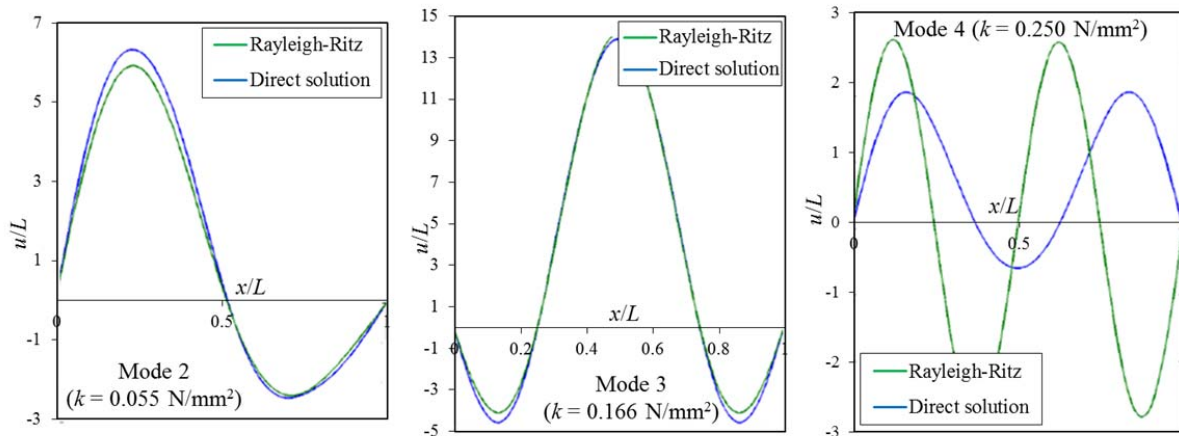
14

Figure 12: Comparison of mode shapes as obtained from direct numerical solution and the Rayleigh–Ritz methods (c_2 = 5 N/mm^3)

5.4 Postbuckling equilibrium paths

The ability of the Fourier series representations of the displacement functions to approximate the full mode shapes accurately is demonstrated again through comparison of the postbuckling paths. In Fig. 13, the load parameter λ is plotted against the end shortening ε to produce equilibrium paths for analyses started along Mode 3. In keeping with the mode shape comparisons of Fig. 12, it can be seen that the truncated Fourier series capture the postbuckling behaviour of the restrained beams quite accurately.
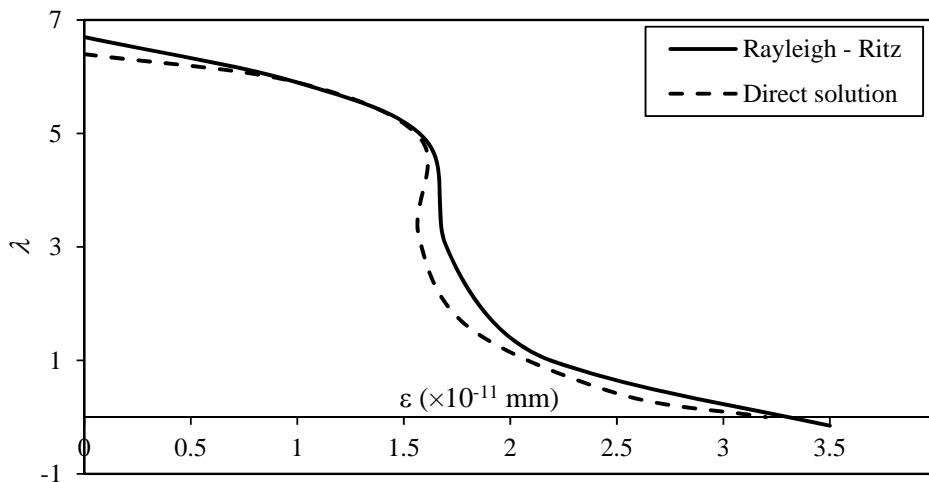

Figure 13: Comparison of equilibrium paths as obtained from direct numerical solution and Rayleigh–Ritz methods for runs started from Mode 3 (k = 0.166 N/mm^2, c_2 = 5 N/mm^3)

6. Conclusions

The postbuckling behaviour of beams provided with a number of discrete restraints with quadratic and cubic nonlinear force–displacement relationships has been investigated. The beam was modelled as simply-supported with a constant bending moment across its span and with a rigid cross-section; thus, there are two degrees-of-freedom or displacement functions: the lateral displacement of the shear

15

centre and the angle of twist. After comparison of the critical moments and deflected shapes obtained for the model using linear restraints with those obtained via equivalent finite element analysis and numerical continuation, respectively, the validity of the form of the potential energy functional was validated. The model was then extended to restraints with nonlinear force–displacement relationships, namely quadratic and cubic relationships.

The governing differential equations of the system were derived via the calculus of variations and solved via numerical continuation methods in AUTO-07p. Results were shown primarily for a beam with three restraints, but these are representative of the overall behaviour of a beam with an arbitrary number of restraints. After determining the variation in critical moment with the linear component of the stiffness, the transition stiffnesses between buckling modes were used as initiation points for further continuations where the nonlinear component of the restraint stiffness is introduced.

It is seen that the degree of instability of the resulting equilibrium paths is generally linked to the strength of the nonlinearity since the restraints are modelled as softening springs. It is also seen that as the load reduces, the deformed shapes tend towards the lower modes. This behaviour is observed for both the quadratic and cubic spring models, but the mode shape itself tends to be non-symmetric for the quadratic model, while there are antisymmetric mode shapes observed in the cubic model, reflecting their respective responses to negative and positive extension.

A Rayleigh–Ritz analysis was performed whereby the displacement functions were represented by truncated Fourier series. Equilibrium equations were derived by minimizing the total potential energy of the system with respect to the amplitudes of the constituent harmonics. It was found that the Fourier series were quite adept at approximating the mode shapes found via direct numerical solution of the governing differential equations for lower modes and at lower stiffnesses. There was also good agreement observed in graphs of critical moment against linear restraint stiffness. At higher stiffnesses and modes, the influence of higher harmonics became apparent.

There is scope for further investigation of this topic, in particular the influence of various forms of nonlinearity in order to model actual restraint behaviour more accurately such material inelasticity in metallic bracing members, buckling of members, cracking in concrete or various nonlinear composite materials. Additionally, further discussion of the nature of the postbuckling equilibrium paths is encouraged.

References
Abaqus (2012). "Abaqus 6.12 manual", Dassault Systemes.

Chrysos, A. (2014). "Lateral torsional buckling in beams with discrete lateral restraints", M.Sc. thesis, Imperial College London, London.

Doedel, E. J., and Oldeman, B. E. (2009). "Auto-07p: Continuation and bifurcation software for ordinary dfferential equations". Tech. Rep., Dept. of Computer Science, Concordia Univ., Montreal, QB, Canada.

Flint, A.R. (1951). "The influence of restraint on the stability of beams". *The Structural Engineer*, 29(9), 235–246.

Hunt, G.W., Wadee, M.A. (1998). "Localization and mode interaction in sandwich structures". *Proceedings of the Royal Society A*, 454(1972), 1197–1216.

McCann, F. (2012). "Stability of beams with discrete lateral restraints." Ph.D. thesis, Imperial College London, London.

McCann, F., Wadee, M.A. and Gardner, L. (2013). "Lateral Stability of Imperfect Discretely Braced Steel Beams". *Journal of Engineering Mechanics, ASCE*, Vol. 139 (2013), 1341–1349.

Pearson, J. (2014). "Nonlinear instability of discretely restrained steel beams", M.Eng. thesis, Imperial College London, London.

Trahair, N. S. (1979). "Elastic lateral buckling of continuously restrained beam columns." The profession of a civil engineer, D. Campbell-Allen and E.H. Davis, eds., Sydney University Press, Sydney, Australia, 61–73.

Trahair, N.S., Nethercot, D.A. (1984). "Bracing requirements in thin walled structures". Chapter 3, Developments in thin-walled structures, J. Rhodes and A.C. Walker, eds., Vol. 2, Elsevier Applied Science Publishers, London, 93–130

Winter, G. (1960). "Lateral bracing of columns and beams". *ASCE Transactions*, 125, 807-826.

Yura, J.A. (2001). "Fundamentals of beam bracing." *AISC Engineering Journal*, 38(1), 11–26.